

Analytical Modeling of Electron Mobility in Strained Germanium

S. Dhar, E. Ungersboeck, H. Kosina, T. Grasser, and S. Selberherr

Institute for Microelectronics, TU Wien, Gußhausstraße 27–29/E360, 1040 Wien, Austria

Phone: +43-1-58801/36018, Fax: +43-1-58801/36099, E-mail: dhar@iue.tuwien.ac.at

Abstract—An analytical model for the low-field bulk electron mobility tensor in strained Germanium is presented. The model includes the effects of strain-induced splitting of the conduction band valleys in Germanium and the corresponding inter-valley scattering reduction as well as temperature and doping dependence. Bulk mobility values larger than 2.5 times the strained Silicon values has been predicted. The results obtained from the model have been verified using Monte Carlo simulations.

I. INTRODUCTION

The introduction of stress in the channel is a well adopted technique for increasing the carrier mobilities in Silicon. Recently, however, the possibility of utilizing Germanium as a channel material [1] [2] [3] is being explored for the next generation CMOS technologies. This interest stems from the significantly higher carrier mobilities in Germanium in comparison to Silicon. In this work, we have investigated the bulk electron mobility in strained Germanium using Monte Carlo simulations and extended a previously suggested analytical low-field mobility model for strained Silicon [4] to calculate the mobility tensor in Germanium as a function of a general stress tensor. The present model is applicable for all stress/strain conditions for which the L -valleys are dominantly populated. The model includes valley splitting for a given strain tensor, the effect of inter-valley scattering, and the doping and temperature dependence.

II. STRAIN EFFECTS ON GERMANIUM BAND STRUCTURE

In Germanium the conduction band minima consist of four degenerate pairs of L -valleys located along the $\langle 111 \rangle$ directions as shown in Fig. 1. Application of strain lifts the degeneracy of the valleys. The valley splitting for the i^{th} valley is calculated using linear deformation potential theory [5]

$$\Delta\epsilon_C^{(i)} = \Xi_d Tr(\hat{\epsilon}) + \Xi_u \mathbf{a}_i^T \cdot \hat{\epsilon} \cdot \mathbf{a}_i$$

$$i = [111], [\bar{1}\bar{1}\bar{1}], [11\bar{1}], [1\bar{1}1] \quad (1)$$

where \mathbf{a}_i is a unit vector of the i^{th} valley-pair minimum and \mathbf{a}_i^T denotes the transposed vector. Ξ_d and Ξ_u are the dilatation and shear deformation potentials, respectively for the L -valleys and $\hat{\epsilon}$ is the strain tensor expressed in the principal coordinate system. The values of Ξ_d and Ξ_u were identified as -4.43 eV and 16.8 eV [6], respectively.

For uniaxial compressive strain along the $[111]$ direction, the L -valleys located along the $[111]$ direction (L_1) are lowered

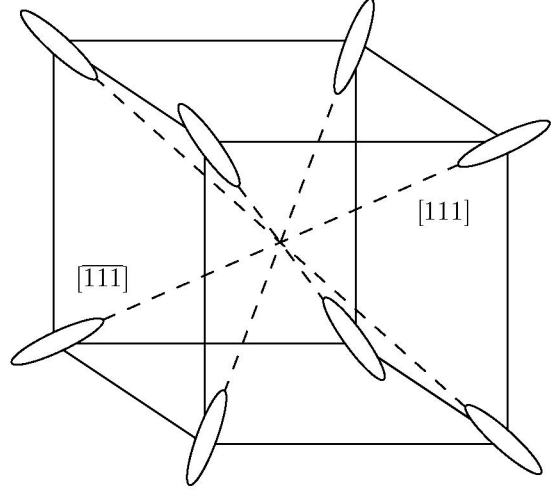


Figure 1: Conduction band structure of unstrained Germanium with constant-energy surfaces for the four equivalent L -valley pairs.

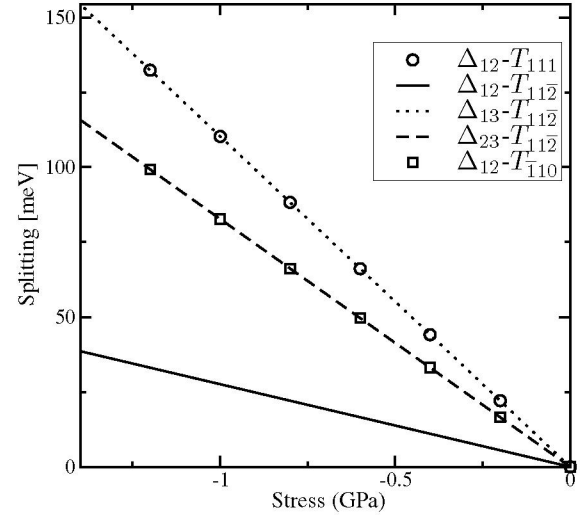


Figure 2: Effect of uniaxial stress on valley splitting ($\Delta_{ij} = \Delta\epsilon_C^{(j)} - \Delta\epsilon_C^{(i)}$) for stress (T) along $[111]$, $[11\bar{2}]$ and $[\bar{1}10]$ directions. T_{hkl} denotes the direction of the applied stress.

in energy, while the remaining three valley pairs (L_2, L_3, L_4) move up in energy and remain degenerate. By this effect, the overall effective mass in the (111) transport plane is lowered and inter-valley phonon scattering is reduced, which results

in a mobility enhancement. Fig. 2 shows the valley splittings, Δ_{ij} , calculated using (1), between initial valley i and final valley j , as a function of stress along $[111]$, $[11\bar{2}]$ and $[\bar{1}10]$ directions. It is observed that for stress along $[11\bar{2}]$ direction, the valleys split into four different energy levels. The figure also indicates that uniaxial stress along $[111]$ direction is most effective in splitting the L-valleys.

III. MODELING

The anisotropic electron mobility tensor for strained Germanium is calculated in the same manner similar proposed for strained Silicon [4]. The electron mobility $\hat{\mu}_{n,\text{str}}^{(i)}$ for the i^{th} conduction band valley in strained Germanium can be expressed as a product of a scalar mobility, μ , and the scaled inverse effective mass tensor, $\hat{m}_{(i)}^{-1}$.

$$\hat{\mu}_{n,\text{str}}^{(i)}(N_I, \Delta\epsilon_C^{(i)}) = \mu \cdot \hat{m}_{(i)}^{-1} \quad (2)$$

$$\mu = \frac{\beta \cdot \mu^L}{1 + (\beta - 1) \cdot h^{(i)} + \beta \cdot \left(\frac{\mu^L}{\mu^{\text{LI}}} - 1 \right)} \quad (3)$$

The scalar mobility is a function of the doping concentration, N_I and the strain induced valley splitting, $\Delta\epsilon_C^{(i)}$. It is calculated taking into account the momentum relaxation times due to acoustic intra-valley scattering and inter-valley scattering between equivalent valleys (g -type) and inter-valley scattering between non-equivalent valleys (f -type scattering), and impurity scattering. The effect of the different scattering mechanisms on the total mobility is estimated by Matthiessen's rule. Symbols μ^L and μ^{LI} signify the lattice mobility and the lattice mobility including the effect of impurity scattering, respectively. The parameter β depends on the mobility enhancement factor, f through

$$\beta = f \cdot \frac{m_t}{m_c}, \quad m_c = \frac{3}{\frac{2}{m_t} + \frac{1}{m_l}}. \quad (4)$$

The mobility enhancement factor is defined as the ratio of the saturation electron mobility in the transversal valleys of strained Germanium to the unstrained mobility. The transversal (m_t) and longitudinal (m_l) effective masses for the ellipsoidal L-valleys in Germanium $m_t = 0.081$ and $m_l = 1.588$, are more anisotropic than those of Silicon.

The scaled inverse effective mass tensor for the i^{th} L-valley in Germanium, $\hat{m}_{(i)}^{-1}$ can be computed using the rotation transformation matrix [7] as follows.

$$\hat{m}_{(i)}^{-1} = U^T \cdot S \cdot U, \quad S = m_c \begin{pmatrix} m_l^{-1} & 0 & 0 \\ 0 & m_t^{-1} & 0 \\ 0 & 0 & m_t^{-1} \end{pmatrix} \quad (5)$$

$$U_{[111]} = \begin{pmatrix} \frac{1}{\sqrt{3}} & \frac{1}{\sqrt{3}} & \frac{1}{\sqrt{3}} \\ -\frac{1}{\sqrt{2}} & \frac{1}{\sqrt{2}} & 0 \\ \frac{-1}{\sqrt{6}} & \frac{-1}{\sqrt{6}} & \frac{\sqrt{2}}{\sqrt{3}} \end{pmatrix} \quad U_{[\bar{1}11]} = \begin{pmatrix} -\frac{1}{\sqrt{3}} & \frac{1}{\sqrt{3}} & \frac{1}{\sqrt{3}} \\ -\frac{1}{\sqrt{2}} & \frac{1}{\sqrt{2}} & 0 \\ \frac{1}{\sqrt{6}} & \frac{-1}{\sqrt{6}} & \frac{\sqrt{2}}{\sqrt{3}} \end{pmatrix}$$

$$U_{[11\bar{1}]} = \begin{pmatrix} -\frac{1}{\sqrt{3}} & -\frac{1}{\sqrt{3}} & \frac{1}{\sqrt{3}} \\ \frac{1}{\sqrt{2}} & -\frac{1}{\sqrt{2}} & 0 \\ \frac{1}{\sqrt{6}} & \frac{1}{\sqrt{6}} & \frac{\sqrt{2}}{\sqrt{3}} \end{pmatrix} \quad U_{[\bar{1}\bar{1}1]} = \begin{pmatrix} \frac{1}{\sqrt{3}} & -\frac{1}{\sqrt{3}} & \frac{1}{\sqrt{3}} \\ \frac{1}{\sqrt{2}} & \frac{1}{\sqrt{2}} & 0 \\ -\frac{1}{\sqrt{6}} & \frac{1}{\sqrt{6}} & \frac{\sqrt{2}}{\sqrt{3}} \end{pmatrix} \quad (6)$$

The inter-valley scattering rate is a function of the strain-induced splitting of the valleys, and lattice temperature, T , and is expressed by a dimensionless factor $h^{(i)}$.

$$h^{(i)} = \frac{g(\Delta_{ij}^{\text{abs}}) + g(\Delta_{il}^{\text{abs}}) + e^{W_{\text{op}}} [g(\Delta_{ij}^{\text{ems}}) + g(\Delta_{il}^{\text{ems}})]}{2[g(-W_{\text{op}}) + \Gamma(\frac{3}{2})]} \quad (7)$$

$$\Delta_{ij}^{\text{abs}} = \frac{\Delta\epsilon_C^{(j)} - \Delta\epsilon_C^{(i)}}{k_B T} - W_{\text{op}} \quad (8)$$

$$\Delta_{ij}^{\text{ems}} = \frac{\Delta\epsilon_C^{(j)} - \Delta\epsilon_C^{(i)}}{k_B T} + W_{\text{op}} \quad (9)$$

$$W_{\text{op}} = \frac{\hbar\omega_{\text{opt}}}{k_B T} \quad (10)$$

The function g is defined as

$$g(z) = \begin{cases} e^{-z} \cdot \Gamma(\frac{3}{2}) & \forall z > 0 \\ e^{-z} \cdot \Gamma(\frac{3}{2}, -z) & \forall z < 0 \end{cases} \quad (11)$$

Here $\hbar\omega_{\text{opt}}$ denotes the phonon energy. $\Gamma(3/2) = \sqrt{\pi}/2$ and $\Gamma(\frac{3}{2}, -z)$ denotes the incomplete Gamma function. The total mobility can then be computed by taking the weighted average of the electron mobility tensor for the i^{th} valley pair, $\hat{\mu}_{n,\text{str}}^{(i)}$ with the corresponding valley population, $p^{(i)}$.

$$\hat{\mu}_{n,\text{str}}^{\text{tot}} = \sum p^{(i)} \cdot \hat{\mu}_{n,\text{str}}^{(i)}, \quad p^{(i)} = \frac{n_{\text{str}}^{(i)}}{\sum n_{\text{str}}^{(i)}},$$

$$n_{\text{str}}^{(i)} = N_C^{(i)} \cdot \exp\left[\frac{\Delta\epsilon_C^{(i)}}{k_B T}\right] \quad (12)$$

Here $n_{\text{str}}^{(i)}$ is calculated for non-degenerate doping concentrations, using Boltzmann statistics with $N_C^{(i)}$ as the effective density of states. In contrast to strained Silicon, the mobility tensor for strained Germanium in (12) is non-diagonal in the principal system due to the non-diagonal nature of the scaled inverse effective mass tensor in (6).

IV. RESULTS AND DISCUSSION

Monte Carlo simulations using [8] were performed and results were compared with those obtained from the analytical model. The Monte Carlo simulations delivered an unstrained value of bulk electron mobility of approximately $3850 \text{ cm}^2/\text{Vs}$ which is close to previously reported values [9] [10].

Fig. 3 shows the variation of the in-plane electron mobility in uniaxially compressively stressed Germanium in the (111) plane as obtained from Monte Carlo simulations. It can

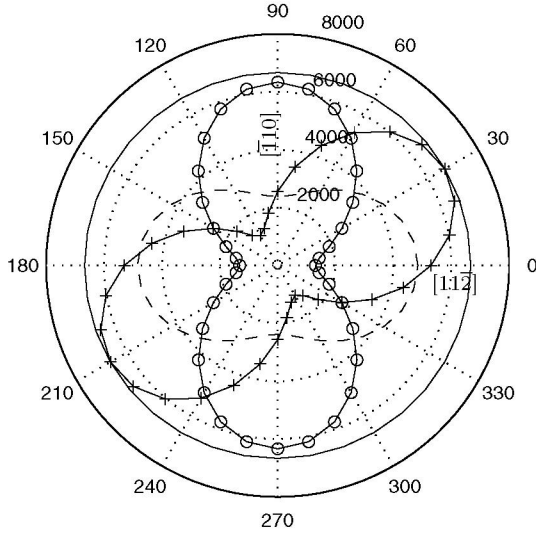


Figure 3: Variation of electron mobility in the (111) plane with the in-plane angle for -1 GPa stress along different directions, at room temperature. Stress directions are represented as: $[111]$ (solid), $[11\bar{2}]$ (solid circle), $[\bar{1}10]$ (dashed) and $[\bar{1}11]$ (solid +).

be clearly observed that uniaxial stress along $[111]$ deliver the highest mobility which is isotropic in the (111) plane. For uniaxial stress along the in-plane directions, the mobility is anisotropic and the enhancement is comparable to that obtained from $[111]$ uniaxial stress.

The computation of the diagonal and non-diagonal components of the mobility tensor in the analytical model requires the calculation of the strain-induced valley splitting. The components of the strain tensor needed to evaluate the splitting for the case of uniaxial stress applied along a general direction can be obtained as follows. We adopt a coordinate system (x', y', z') in which the stress tensor has only one non-zero component, σ'_{xx} . The stress tensor from this coordinate system is transformed to the principal coordinate system using the transformation matrix [11]. The strain components in the principal system are then obtained by inversion of Hook's law. After the mobility tensor is obtained in the principal system, the mobility along a particular direction can be calculated from (12) by taking the projection of the tensor in that direction.

Fig. 4 and Fig. 5 show the analytically calculated electron mobility components for uniaxial compressive and tensile stresses, respectively. Also shown for comparison are the

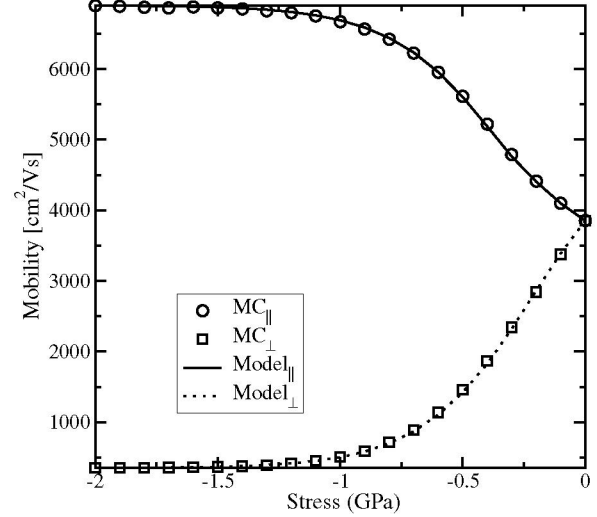


Figure 4: Electron mobility components in (111) plane versus uniaxial compressively (along $[111]$) stress at room temperature. $MC_{||}$ indicates the isotropic in-plane mobility, while MC_{\perp} denotes the out-of-plane mobility.

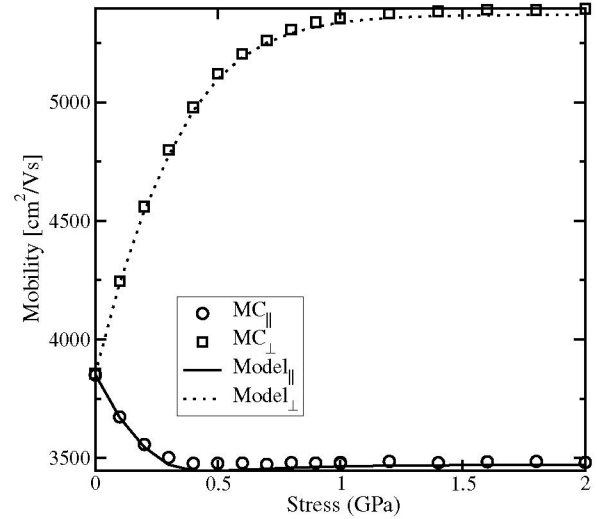


Figure 5: Electron mobility in (111) plane versus uniaxial tensile (along $[111]$) stress at room temperature. $MC_{||}$ indicates the isotropic in-plane mobility, while MC_{\perp} denotes the out-of-plane mobility.

Monte Carlo simulation results (symbols). Fig. 4 indicates that the application of compressive stress increases the electron mobility in the (111) plane with the mobility value saturating at $6900 \text{ cm}^2/\text{Vs}$ for stress values greater than -1.5 GPa . This mobility improvement is nearly 2.8 times the enhanced bulk mobility in strained Silicon. On the contrary, applying uniaxial tensile stress along $[111]$ direction results in larger out-of-plane mobilities, shown in Fig. 5.

In order to see the effect of temperature on the mobility, we calculated the unstrained and strained (-3 GPa) electron

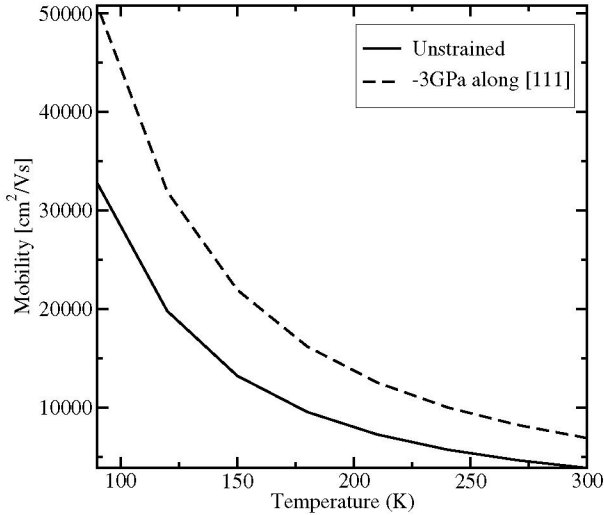


Figure 6: Electron mobility in the (111) plane as a function of temperature for unstrained and -3 GPa (along [111] direction) strained Germanium.

mobilities from Monte Carlo simulations for different temperatures ranging from 300K to 90K, as shown in Fig. 6. It was found that the temperature dependence of both the unstrained as well as strained mobilities can be fit using a power law expression.

$$\mu = \mu_{300} (300/T)^\alpha \quad (13)$$

Here $\mu_{300} = 3850 \text{ cm}^2/\text{Vs}$ is the unstrained bulk mobility at 300K and value of parameter $\alpha = 1.78$ has been extracted from the Monte Carlo data. Finally, the temperature dependence is introduced into the analytical model through the enhancement factor f as

$$f = f_{300} (300/T)^\beta \quad (14)$$

where f_{300} is the mobility enhancement in unstrained Germanium at 300K. The values of f_{300} and β were chosen as 1.79 and -0.12 , respectively. The variation in lattice temperature also affects the mobility through the inter-valley scattering rate (Eq. (7)-(10)) and the valley populations (Eq. (12)). Fig. 7 shows a comparison of the mobility components in the (111) plane for increasing level of compressive stress along [111] direction at lattice temperature $T = 200\text{K}$, as obtained from Monte Carlo simulations and the model. It can be seen that the agreement is very good.

V. CONCLUSION

An analytical model has been developed to describe the anisotropy of the electron mobility in strained Germanium. The model includes the temperature and doping dependence and the effect of reduced inter-valley scattering due to valley splitting. Results obtained from the model show very good

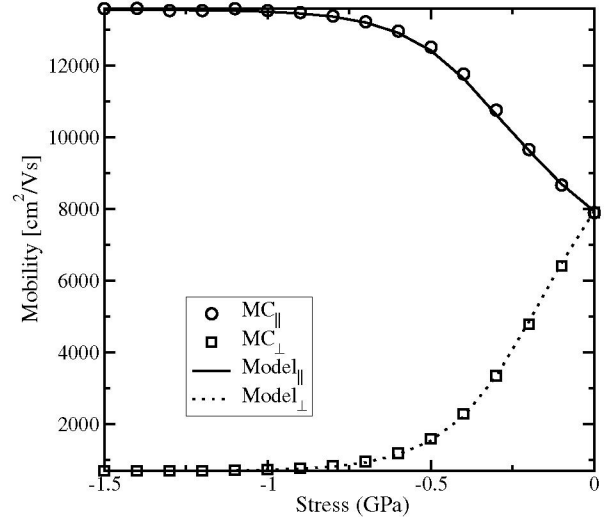


Figure 7: Electron mobility in the (111) plane versus uniaxial compressive stress along [111] at 200K. $MC_{||}$ indicates the isotropic in-plane mobility, while MC_{\perp} denotes the out-of-plane mobility.

agreement with MC simulations for both uniaxial compressive and tensile stress conditions. The model is suitable for implementation in TCAD device simulators.

ACKNOWLEDGMENT

We acknowledge financial support through the European Commission for project D-DOTFET, 012150-2.

REFERENCES

- [1] C. W. Liu, S. Maikap, and C. Y. Yu, *IEEE Circuits and Devices Magazine* **21**, 21 (2005).
- [2] T. Low *et al.*, *Appl.Phys.Lett.* **85**, 2402 (2004).
- [3] C. Yeo *et al.*, *IEEE Electron Device Lett.* **26**, 761 (2005).
- [4] S. Dhar *et al.*, *IEEE Trans.Electron Devices* **52**, 527 (2005).
- [5] I. Balslev, *Physical Review* **143**, 636 (1966).
- [6] M. Fischetti and S. Laux, *J.Appl.Phys.* **80**, 2234 (1996).
- [7] C. Herring and E. Vogt, *Phys.Rev.* **101**, 944 (1956).
- [8] *VMC 1.0 User's Guide*, Technische Universität Wien, Austria, 2004.
- [9] M. B. Prince, *Phys.Rev.* **92**, 681 (1953).
- [10] F. J. Morin, *Phys.Rev.* **93**, 62 (1954).
- [11] S. Smirnov and H. Kosina, *Solid State Electronics* **48**, 1325 (2004).